

Ulrasmall Sn Nanoparticles Embedded in Nitrogen-Doped Porous Carbon As High-Performance Anode for Lithium-Ion Batteries

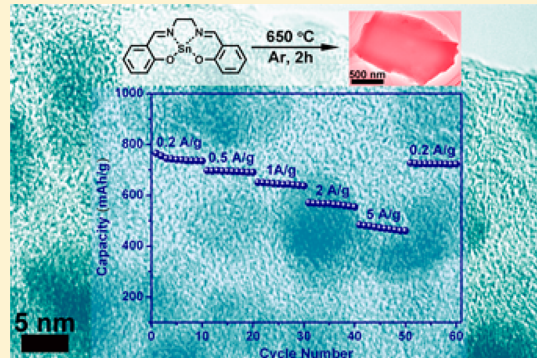
Zhiqiang Zhu, Shiwen Wang, Jing Du, Qi Jin, Tianran Zhang, Fangyi Cheng, and Jun Chen*

Key Laboratory of Advanced Energy Materials Chemistry (Ministry of Education), College of Chemistry; Collaborative Innovation Center of Chemical Science and Engineering, Nankai University, Tianjin 300071, China

Supporting Information

ABSTRACT: In this Letter, we reported on the preparation and Li-ion battery anode application of ulrasmall Sn nanoparticles (~ 5 nm) embedded in nitrogen-doped porous carbon network (denoted as 5-Sn/C). Pyrolysis of Sn(Salen) at 650 °C under Ar atmosphere was carried out to prepare N-doped porous 5-Sn/C with the BET specific surface area of $286.3\text{ m}^2\text{ g}^{-1}$. The 5-Sn/C showed an initial discharge capacity of 1014 mAh g^{-1} and a capacity retention of 722 mAh g^{-1} after 200 cycles at the current density of 0.2 A g^{-1} . Furthermore, a reversible capacity of $\sim 480\text{ mAh g}^{-1}$ was obtained at much higher current density of 5 A g^{-1} . The remarkable electrochemical performance of 5-Sn/C was attributed to the effective combination of ulrasmall Sn nanoparticles, uniform distribution, and porous carbon network structure, which simultaneously solved the major problems of pulverization, loss of electrical contact, and particle aggregation facing Sn anode.

KEYWORDS: Tin nanoparticles, nitrogen-doped porous carbon network, Sn (Salen), anode, Li-ion battery



Lithium ion batteries (LIBs) have attracted increasing attention in the areas of electrochemical energy storage for mobile and stationary applications due to their high energy density and long cycle life.^{1–3} However, the prevailing commercial anode material, graphite, is far from meeting the requirements for high energy/power density because of its low theoretical capacity (372 mAh g^{-1}).^{4–6} Therefore, much effort has been devoted to developing anode materials with high capacity, long cycling stability, and high rate capability.^{7–9} In this regard, metallic tin (Sn), which shows a high theoretical capacity (ca. 992 mAh g^{-1} for $\text{Li}_{4.4}\text{Sn}$) and an appropriate low discharge potential versus Li/Li^+ , has been considered as one of the most promising alternative anode materials for next generation LIBs.^{10–12} However, the practical application of Sn suffers from its pulverization problem caused by the huge volume change during lithiation/delithiation processes, which would result in the loss of electrical conductivity and consequently a rapid capacity fading in the cycling.^{13,14}

Previous reports have shown that decreasing the dimension of Sn into nanometer range could reduce the mechanical stress generated during lithiation/delithiation and, thus, inhibit the tendency for fracture and decrepitation.^{15,16} In addition, the nanostructure could shorten the path lengths for Li-ion transport, providing high rate capability.^{17,18} However, the cyclability is still limited due to the aggregation of Sn nanoparticles (NPs).¹⁹ To simultaneously tackle all these problems, various Sn/C nanocomposites have been fabricated, displaying improved electrochemical performance than that of bare nano-Sn.^{20–24} For example, Scrosati and co-workers

showed that a Sn/C composite electrode could provide a stable capacity of 500 mAh g^{-1} for several hundreds of cycles.²⁰ The carbon matrix not only acts as a buffer to accommodate the volume expansion, but also prevents particle aggregation. Yu's group demonstrated that Sn particles encapsulated in porous multichannel carbon microtubes could obtain a reversible capacity of 648 mAh g^{-1} after 140 cycles.²¹ The porous carbon shell is responsible for the improved electrode performance. More recently, Sn NPs uniformly dispersed in a spherical carbon matrix has been synthesized by a spray pyrolysis technique, showing a capacity of 710 mAh g^{-1} after 130 cycles at 0.2 A g^{-1} .²⁴ The remarkable performance is attributed to the small particle size (~ 10 nm) and uniform distribution of Sn NPs. Definitely, small particle size, uniform distribution, and porous network structure are the key factors for Sn/C composite to achieve high electrochemical performance. However, fabrication of such Sn/C composite containing the three features is rarely reported and remains a big challenge.

Herein, we reported a facile, straightforward one-pot synthesis of ulrasmall Sn NPs (with typical size of ~ 5 nm, denoted as 5-Sn/C) finely embedded in N-doped porous carbon network by carbonizing divalent Sn complex, Sn(Salen). In contrast with previous methods that require mixing tin and carbon sources, the two sources are combined in one molecule, Sn(Salen), which contains a Sn atom located above the $[\text{N}_2\text{O}_2]$

Received: September 29, 2013

Revised: November 24, 2013

Published: December 11, 2013



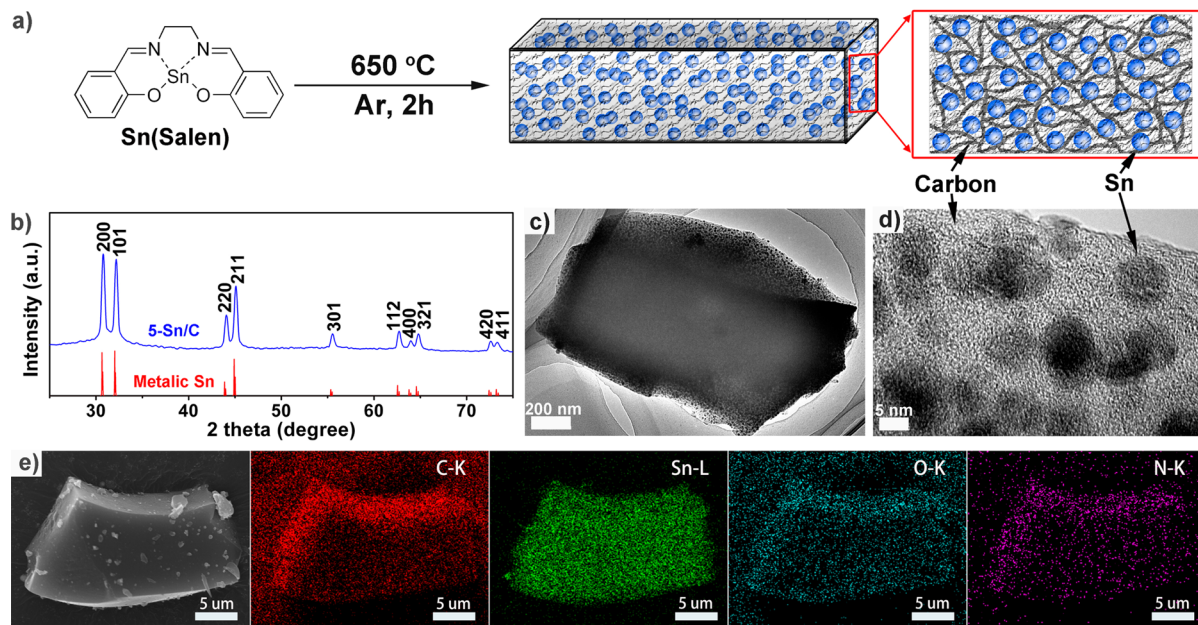


Figure 1. (a) Synthesis procedure and schematic diagram, (b) XRD patterns of 5-Sn/C and metallic Sn (JCPDS card No. 04-0673), (c) TEM image, (d) HRTEM image, (e) SEM and EDS mapping images of ultrasmall Sn NPs dispersed in N-doped porous carbon matrix (5-Sn/C).

plane of the salen ligand (Figure 1a). As a result, Sn is homogeneously distributed in the organic framework at molecular dimension. During the pyrolysis process, the salen ligand is transformed to a porous carbon network while the metal cation is *in situ* reduced to uniform Sn nanoparticles (~ 5 nm), generating the final Sn/C composite. In addition, partial N species in the precursor could be reserved in the composite, forming N-doped porous carbon network and hence providing high conductivity.^{25,26} Such unique structure endues the composite with excellent electrochemical performance as an anode material for LIBs.

The Sn/C composite was synthesized by simply carbonizing of divalent Sn complex, Sn(Salen). The preparation of Sn(Salen) precursor was described in Supporting Information according to previously reported procedures.²⁷ Instrumental analyses such as IR (Supporting Information Figure S1), NMR (Supporting Information Figure S2), and elemental analysis were used to characterize the structure of the as-prepared Sn(Salen). All results suggest the successful synthesis of high-purity target molecule. Pyrolysis of Sn(Salen) at 650 °C under Ar atmosphere gave the N-doped porous Sn/C composite. Figure 1b shows the X-ray diffraction (XRD) patterns of the as-prepared composite and metallic Sn. All diffraction peaks can be readily indexed to crystalline tin (JCPDS card No. 04-0673). No intensive peak belonging to carbon is detected, demonstrating the amorphous nature of carbon.²⁸ This is supported by the Raman spectrum of the 5-Sn/C sample (Supporting Information Figure S3), in which two broad peaks at 1338 and 1590 cm⁻¹ can be assigned to typical D and G bands of amorphous carbon, respectively.²⁹ Generally, amorphous carbon contains abundant defects and vacancies, which not only favor the diffusion of lithium ions, but also provide more reversible sites for Li storage, contributing to the overall capacity.^{30–32} The chemical composition at the surface of 5-Sn/C composite was investigated by X-ray photoelectron spectroscopy (XPS). The Sn 3d spectra (Supporting Information Figure S4a) shows two characteristic peaks at 487.3 eV (Sn 3d_{5/2}) and 495.7 eV (Sn 3d_{3/2}), indicating that

some Sn NPs near the surface of the carbon matrix were oxidized to SnO₂.³³ The existence of Sn–O bonding was also confirmed by the high-resolution O1s XPS spectrum of 5-Sn/C as shown in Supporting Information Figure S4b. Besides, the peak corresponded to C–O bonding was also observed. Furthermore, combined with the O1s spectrum of salen-C synthesized by prolysis of salen-H₂ ligand (Supporting Information Figure S4c), the results indicated that the presence of oxygen is ascribed to both the carbon matrix and SnO₂. Nevertheless, the presented SnO₂ could improve the total capacity of the composite as the reduction of SnO₂ to Sn corresponds to a high theoretical capacity of 1494 mAh g⁻¹.³⁴ In addition, a small peak located at around 400 eV originated from N 1s was found in the full XPS spectrum of 5-Sn/C, suggesting the formation of N-doped carbon matrix. Elemental analysis also illustrates that the as-prepared 5-Sn/C composite possesses 4.6 wt % N species. It is believed that N-doping can enhance the electric conductivity of carbon based material and thus improve the electrochemical performance.²⁵ The tin content of 5-Sn/C composite determined from the thermogravimetric analysis (TGA, Supporting Information Figure S5) was approximately 58 wt %. The loading of Sn is comparable with other reported Sn/C composites.^{24,29,35}

The morphology of the as-prepared 5-Sn/C composite was characterized using transmission electron microscopy (TEM).^{36,37} As shown in Figure 1c, Sn NPs (black dots) with uniform particle size were homogeneously embedded in the carbon framework (gray matrix). The typical size of Sn particles is around 5 nm, which could be clearly seen from the high-resolution TEM (HRTEM) image (Figure 1d). The energy dispersive spectrometer (EDS) mapping (Figure 1e) of the as-made sample demonstrates that Sn NPs are highly dispersed in the carbon matrix. Besides tin and carbon, oxygen and nitrogen were also detected, being consistent with the XPS result. However, it should be noted that most of Sn NPs were wrapped in the carbon network rather than exposed on the outer surface. As a result, the carbon matrix not only prevents the aggregation of tin particles, but also avoids the exfoliation of

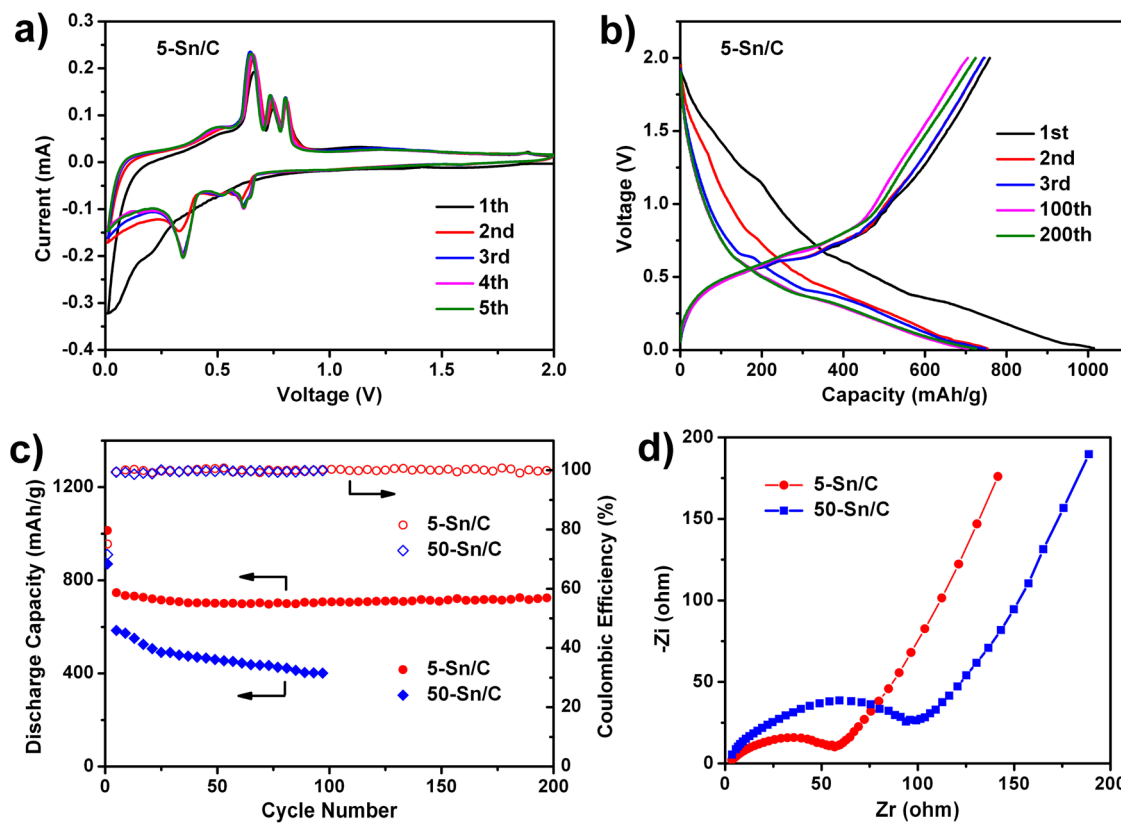


Figure 2. (a) Cyclic voltammetry curve of 5-Sn/C electrode at 0.1 mV s^{-1} scanning rate. (b) Galvanostatic charge–discharge profiles of 5-Sn/C electrode at a constant current density of 0.2 A g^{-1} . (c) Cycling performance of 5-Sn/C and 50-Sn/C electrodes at 0.2 A g^{-1} . (d) Electrochemical impedance spectra of the two nano-Sn/C electrodes collected at 0.3 V after five cycles.

Sn NPs during lithiation/delithiation, maintaining the integrity of the whole electrode. In addition, much free space would be produced due to the release of gases during the carbonization of the organic framework and the volume contraction of molten Sn upon the cooling process (Sn metal has a low melting point of 232°C),²⁰ as proved by N_2 adsorption–desorption analysis (Supporting Information Figure S6). The isotherm with a steep increase at low relative pressures is typical type-I behavior, implying that the composite contains a large amount of micropores.³⁸ Accordingly, the composite possess a large BET specific surface area of $286.3 \text{ m}^2 \text{ g}^{-1}$. During the discharge/charge process, the porous structure allows for the expansion of Sn without mechanical constrains, prevents it from loosing contact with the current collector, and fascinates diffusion of lithium ions through the carbon matrix.³⁹ All of these results demonstrate that the as-prepared Sn/C composite encompasses three key advantages of ultrasmall Sn nanoparticles, uniform distribution, and porous carbon network structure.

The unique morphology and structure of the as-prepared porous Sn/C network composite motivate us to further investigate its electrode performance. For comparison, another Sn/C composite with average Sn particle size of $\sim 50 \text{ nm}$ without a uniform shape was prepared at 700°C (denoted as 50-Sn/C, Supporting Information Figure S7). The large particle size arose from the irregular ripening of Sn NPs under high temperature.⁴⁰ Element analysis reveals that N species is also present in 50-Sn/C. However, the N content of 2.2 wt % is lower than that in 5-Sn/C. Electrochemical measurements of the two composites were performed with coin-type cells that employ lithium foil as both reference and counter electrodes

and 1 M LiPF₆ ethylene carbonate-diethyl carbonate (EC/DEC) solution as the electrolyte. The working electrode consists of 80 wt % active material, 10 wt % super P, and 10 wt % sodium carboxymethyl cellulose (CMC) binder. The loading amount of the active material for the electrode is about 1.4 mg cm^{-2} . Figure 2a shows the typical cyclic voltammograms (CVs) of 5-Sn/C electrode in the initial five cycles at a scan rate of 0.1 mV s^{-1} between 0 and 2 V. During the first cathodic sweep, the broad reduction peak from 0.7 to 0.1 V is ascribed to both the reduction of Sn and the decomposition of the electrolyte to form solid-electrolyte interphase (SEI) film, corresponding to the capacity loss during the first cycle.⁴¹ However, from the second cycle onward, only three distinct peaks that are centered at 0.34, 0.51, and 0.62 V can be found, being originated from the formation of Li_xSn alloy.⁴² In the anodic sweep, oxidation peaks between 0.4 and 0.9 V are assigned to the dealloying reaction of Li_xSn .²⁴ All peaks are reproducible and stable after the first cycle, implying the reversibility of the electrochemical reactions of 5-Sn/C electrode. Additionally, the absence of peaks associated to the catalytic decomposition of the electrolyte on metallic Sn (at 1.05 or 1.55 V) verified that Sn nanoparticles were well embedded in the porous carbon network.^{42,43}

Figure 2b displays the voltage profiles of 5-Sn/C anode in different cycles between 0.01 and 2.0 V at a current density of 0.2 A g^{-1} . The voltage profiles are typical characteristics of a Sn electrode.⁴⁴ Unless stated, all the specific capacity values reported in this paper are calculated on the basis of the total mass of Sn/C composite. The first discharge and charge capacities of 5-Sn/C are 1014 and 757 mAh g^{-1} , respectively,

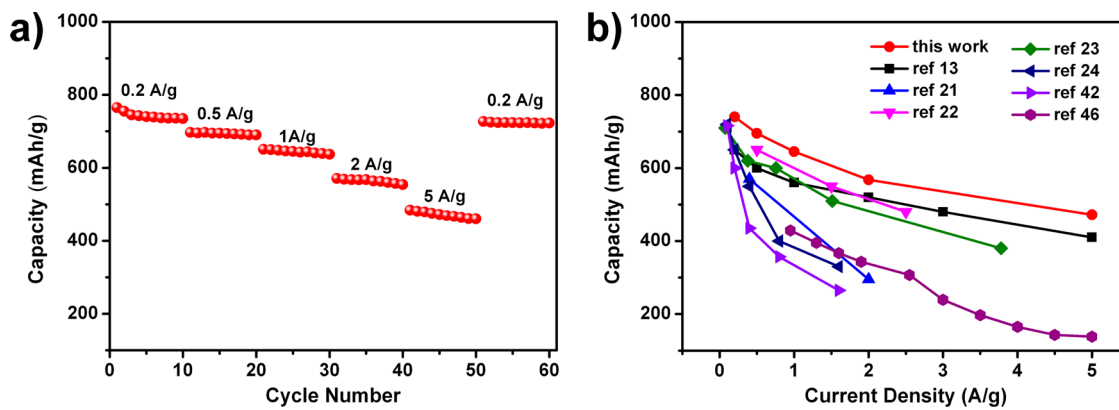


Figure 3. (a) Rate capability of 5-Sn/C composite anode and (b) this work with the comparison to previously reported Sn/C composites.

corresponding to a Coulombic efficiency (CE) of 75%. This high CE indicates that the embedment of Sn NPs in the carbon matrix can largely avoid detrimental reactions between Sn and electrolyte, in good agreement with the CV result. The high capacity should benefit from the ultrasmall particles of Sn NPs and porous carbon network structure, which enables the full utilization of Sn NPs. More importantly, after several cycles the reversible capacity is stabled at ~ 720 mAh g $^{-1}$. The slow shrinkage of charge/discharge curves after the first cycle implies the high cycling stability of the as-prepared composite. For comparation, 50-Sn/C composite anode delivered an initial discharge capacity of 870 mAh g $^{-1}$ with a CE of 71% (Supporting Information Figure S8). The high initial irreversible capacity is ascribed to the severe SEI formation on the surface of 50-Sn/C composite. Additionally, the discharge curve of 50-Sn/C contracts fast upon cycling, meaning an ineffective contact and then a faster capacity decay.

Figure 2c shows the cycling performance of 5-Sn/C and 50-Sn/C composite electrodes. It is clearly seen that 5-Sn/C electrode exhibits much better cycling stability than that of 50-Sn/C electrode. After 200 cycles, 5-Sn/C anode still delivered a capacity of 722 mAh g $^{-1}$, which is nearly 2 times higher than that of traditional graphitic anode (~ 372 mAh g $^{-1}$). This result is also superior to those for Sn/C composites reported previously.^{13,21,22,24} The capacity fading in the initial several cycles may be derived from the partial irreversible insertion of lithium ions into the vacancies of the porous carbon matrix.³¹ However, it should be pointed out that a high CE of >99% was achieved after several cycles, demonstrating high reversibility of 5-Sn/C anode. On the other hand, only a low capacity of 397 mAh g $^{-1}$ has been maintained for 50-Sn/C anode after 100 cycles. The particle aggregation or pulverization caused by the large volume expansion during lithiation/delithiation processes should account for the rapid capacity decay of 50-Sn/C anode, as confirmed by the TEM analysis of 50-Sn/C electrode after 100 cycles (Supporting Information Figure S9).

Figure 2d displays the impedance spectra of the two Sn/C composites. The resistance of 5-Sn/C electrode is much lower than that of 50-Sn/C electrode, which should be derived from the higher N-doping level of 5-Sn/C composite compared with that of 50-Sn/C composite.⁴⁵ As a sum result, the much better cyclability of 5-Sn/C composite is attributed to the following several merits. First, the ultrasmall size of Sn NPs could significantly reduce the strain generated during the lithiation/delithiation processes and then suppress the fracture of Sn NPs. Second, on account of the homogeneous dispersion of Sn NPs, the generated stress upon cycling would evenly distribute in the

whole composite as well as the electrode, preventing local cracking. Finally, the porous carbon network structure not only prevents particle aggregation, but also renders sufficient void space, allowing the volume expansion/contraction of Sn NPs and thus maintaining the structural integrity and electrical conductivity of the electrode. These unique features make 5-Sn/C composite a very promising anode material for LIBs.

Figure 3a shows the rate performance of a 5-Sn/C composite anode cycled at various current densities from 0.2 to 5 A g $^{-1}$. The corresponding charge–discharge profiles are given in Supporting Information Figure S10. The specific reversible capacity of the sample falls moderately with increasing current density. At a low current density of 0.2 A g $^{-1}$, the specific reversible capacity reaches ~ 740 mAh g $^{-1}$. Even at a higher current density of 5 A g $^{-1}$, it delivers a capacity of ~ 480 mAh g $^{-1}$, which is still higher than the practical capacity obtained from commercial graphite. This result compares favorably with previously reported Sn/C composites (Figure 3b).^{13,21–24,42,46} The superior rate capability of 5-Sn/C nanostructure should benefit from the combination of the high electric conductivity offered by N-doped carbon matrix and the short diffusion path for both electrons and ions provided by the ultrasmall Sn particles and the porous carbon network structure. Besides, the cell capacity could recover to the original values when the current density returns to lower current density after high rate cycling, indicating that the unique structure of 5-Sn/C composite could preserve the integrity of the electrode and thus tolerant to varied charge and discharge currents, which is important for high power applications of rechargeable batteries.

To further understand the outstanding electrochemical performance of 5-Sn/C composite, TEM analysis has been performed to observe the morphological change of the electrode after 200 charge/discharge cycles at 0.2 A g $^{-1}$. It is clearly seen from Figure 4 that the composite anode still retains its original appearance (as shown in Figure 1b,c) even after

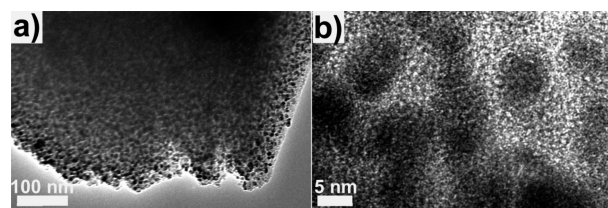


Figure 4. (a) TEM and HRTEM (b) images of 5-Sn/C composite after 200 charge/discharge cycles.

long time cycling. Notably, all Sn NPs are uniformly confined in the carbon matrix, further certifying that the unique structure of the composite effectively alleviates the pulverization and prevents the particle aggregation, thus ensuring the long cycle stability.

In conclusion, Sn/C composite with ultrasmall Sn nanoparticles (~ 5 nm) delicately dispersed in N-doped porous carbon network was prepared by pyrolysis of Sn(Salen) and further evaluated as anode material for rechargeable Li-ion batteries. It is demonstrated that as the anode of LIBs, S-Sn/C composite with the combination of ultrasmall Sn nanoparticles, uniform distribution and porous carbon network structure render long cycling stability and high rate capability. At a current density of 0.2 A g^{-1} , a capacity of $\sim 722 \text{ mAh g}^{-1}$ was maintained after 200 cycles. Even at much higher current density of 5 A g^{-1} , a reversible capacity of $\sim 480 \text{ mAh g}^{-1}$ was obtained. These results would shed light on the practical application of Sn-based materials as high capacity electrode with high rate capability for next generation LIBs.

■ ASSOCIATED CONTENT

Supporting Information

Detailed experimental procedures, and additional materials characterization. This material is available free of charge via the Internet at <http://pubs.acs.org>.

■ AUTHOR INFORMATION

Corresponding Author

*E-mail: chenabc@nankai.edu.cn.

Notes

The authors declare no competing financial interest.

■ ACKNOWLEDGMENTS

This work was supported by the Programs of National (973 (2011CB935900), NSFC (51231003 and 21322101), and MOE (B12015 and 113016A).

■ REFERENCES

- (1) Armand, M.; Tarascon, J. M. *Nature* **2008**, *451*, 652.
- (2) Chen, J.; Cheng, F. Y. *Acc. Chem. Res.* **2009**, *42*, 713.
- (3) Xin, S.; Guo, Y. G.; Wan, L. *J. Acc. Chem. Res.* **2012**, *45*, 1759.
- (4) Idota, Y.; Kubota, T.; Matsufuji, A.; Maekawa, Y.; Miyasaka, T. *Science* **1997**, *276*, 1395.
- (5) Park, M. H.; Kim, M. G.; Joo, J.; Kim, K.; Kim, J.; Ahn, S.; Cui, Y.; Cho, J. *Nano Lett.* **2009**, *9*, 3844.
- (6) Chen, X. L.; Li, X. L.; Ding, F.; Xu, W.; Xiao, J.; Cao, Y. L.; Meduri, P.; Liu, J.; Graff, G. L.; Zhang, J. G. *Nano Lett.* **2012**, *12*, 4124.
- (7) Ma, H.; Cheng, F. Y.; Chen, J.; Zhao, J. Z.; Li, C. S.; Tao, Z. L.; Liang, J. *Adv. Mater.* **2007**, *19*, 4067.
- (8) Wang, Z. Y.; Luan, D. Y.; Boey, F. Y. C.; Lou, X. W. *J. Am. Chem. Soc.* **2011**, *133*, 4738.
- (9) Wu, H.; Yu, G. H.; Pan, L. J.; Liu, N.; McDowell, M. T.; Bao, Z. N.; Cui, Y. *Nat. Commun.* **2013**, *4*, 1943.
- (10) Zou, Y. Q.; Wang, Y. *ACS Nano* **2011**, *5*, 8108.
- (11) Kim, M. G.; Sim, S.; Cho, J. *Adv. Mater.* **2010**, *22*, 5154.
- (12) Hu, R. Z.; Shi, Q.; Wang, H.; Zeng, M. Q.; Zhu, M. *J. Phys. Chem. C* **2009**, *113*, 18953.
- (13) Ji, L. W.; Tan, Z. K.; Kuykendall, T.; An, E. J.; Fu, Y. B.; Battaglia, V.; Zhang, Y. G. *Energy Environ. Sci.* **2011**, *4*, 3611.
- (14) Cui, L. F.; Shen, J.; Cheng, F. Y.; Tao, Z. L.; Chen, J. *J. Power Sources* **2011**, *196*, 2195.
- (15) Besenhard, J. O.; Yang, J.; Winter, M. *J. Power Sources* **1997**, *68*, 87.
- (16) Kravchyk, K.; Protesescu, L.; Bodnarchuk, M. I.; Krumeich, F.; Yarema, M.; Walter, M.; Guntlin, C.; Kovalenko, M. V. *J. Am. Chem. Soc.* **2013**, *135*, 4199.
- (17) Zhang, X. L.; Cheng, F. Y.; Yang, J.; Chen, J. *Nano Lett.* **2013**, *13*, 2822.
- (18) Wang, S. W.; Wang, L. J.; Zhang, K.; Zhu, Z. Q.; Tao, Z. L.; Chen, J. *Nano Lett.* **2013**, *13*, 4404.
- (19) Guo, B. K.; Shu, J.; Tang, K.; Bai, Y.; Wang, Z. X.; Chen, L. Q. *J. Power Sources* **2008**, *177*, 205.
- (20) Derrien, G.; Hassoun, J.; Panero, S.; Scrosati, B. *Adv. Mater.* **2007**, *19*, 2336.
- (21) Yu, Y.; Gu, L.; Zhu, C. B.; van Aken, P. A.; Maier, J. *J. Am. Chem. Soc.* **2009**, *131*, 15984.
- (22) Yu, Y.; Gu, L.; Wang, C. L.; Dhanabalan, A.; van Aken, P. A.; Maier, J. *Angew. Chem., Int. Ed.* **2009**, *48*, 6485.
- (23) Luo, B.; Wang, B.; Liang, M.; Ning, J.; Li, X.; Zhi, L. *Adv. Mater.* **2012**, *24*, 1405.
- (24) Xu, Y. H.; Liu, Q.; Zhu, Y. J.; Liu, Y. H.; Langrock, A.; Zachariah, M. R.; Wang, C. S. *Nano Lett.* **2013**, *13*, 470.
- (25) Qie, L.; Chen, W. M.; Wang, Z. H.; Shao, Q. G.; Li, X.; Yuan, L. X.; Hu, X. L.; Zhang, W. X.; Huang, Y. H. *Adv. Mater.* **2012**, *24*, 2047.
- (26) Wu, Z. S.; Ren, W. C.; Xu, L.; Li, F.; Cheng, H. M. *ACS Nano* **2011**, *5*, 5463.
- (27) Jing, H. W.; Edulji, S. K.; Gibbs, J. M.; Stern, C. L.; Zhou, H. Y.; Nguyen, S. T. *Inorg. Chem.* **2004**, *43*, 4315.
- (28) Deng, D.; Lee, J. Y. *Angew. Chem., Int. Ed.* **2009**, *48*, 1660.
- (29) Hwang, J.; Woo, S. H.; Shim, J.; Jo, C.; Lee, K. T.; Lee, J. *ACS Nano* **2013**, *7*, 1036.
- (30) Zheng, T.; Zhong, Q.; Dahn, J. R. *J. Electrochem. Soc.* **1995**, *142*, L211.
- (31) Kim, I. S.; Blomgren, G. E.; Kumta, P. N. *Electrochem. Solid-State Lett.* **2004**, *7*, A44.
- (32) Zhu, Z. Q.; Cheng, F. Y.; Chen, J. *J. Mater. Chem. A* **2013**, *1*, 9484.
- (33) Wang, L.; Wang, D.; Dong, Z. H.; Zhang, F. X.; Jin, J. *Nano Lett.* **2013**, *13*, 1711.
- (34) Zhou, X.; Wan, L. J.; Guo, Y. G. *Adv. Mater.* **2013**, *25*, 2152.
- (35) Hassoun, J.; Derrien, G.; Panero, S.; Scrosati, B. *Adv. Mater.* **2008**, *20*, 3169.
- (36) Cheng, F. Y.; Shen, J.; Peng, B.; Pan, Y. D.; Tao, Z. L.; Chen, J. *Nat. Chem.* **2011**, *3*, 79.
- (37) Cheng, F. Y.; Zhang, T. R.; Zhang, Y.; Du, J.; Han, X. P. *Angew. Chem., Int. Ed.* **2013**, *52*, 2474.
- (38) Palaniselvam, T.; Biswal, B. P.; Banerjee, R.; Kurungot, S. *Chem.—Eur. J.* **2013**, *19*, 9335.
- (39) Wu, X. L.; Jiang, L. Y.; Cao, F. F.; Guo, Y. G.; Wan, L. J. *Adv. Mater.* **2009**, *21*, 2710.
- (40) Yang, S. J.; Nam, S.; Kim, T.; Im, J. H.; Jung, H.; Kang, J. H.; Wi, S.; Park, B.; Park, C. R. *J. Am. Chem. Soc.* **2013**, *135*, 7394.
- (41) Li, W.; Yang, R.; Zheng, J.; Li, X. G. *Nano Energy* **2013**, *2*, 1314.
- (42) Luo, B.; Wang, B.; Li, X. L.; Jia, Y. Y.; Liang, M. H.; Zhi, L. J. *Adv. Mater.* **2012**, *24*, 3538.
- (43) Jung, Y. S.; Lee, K. T.; Ryu, J. H.; Im, D.; Oh, S. M. *J. Electrochem. Soc.* **2005**, *152*, A1452.
- (44) Xu, L. P.; Kim, C.; Shukla, A. K.; Dong, A.; Mattox, T. M.; Milliron, D. J.; Cabana, J. *Nano Lett.* **2013**, *13*, 1800.
- (45) Ren, W.; Li, D.; Liu, H.; Mi, R.; Zhang, Y.; Dong, L. *Electrochim. Acta* **2013**, *105*, 75.
- (46) Meschini, I.; Nobili, F.; Mancini, M.; Marassi, R.; Tossici, R.; Savoini, A.; Focarete, M. L.; Croce, F. *J. Power Sources* **2013**, *226*, 241.